KeAi

CHINESE ROOTS
GLOBAL IMPACT

Contents lists available at ScienceDirect

Petroleum Science

journal homepage: www.keaipublishing.com/en/journals/petroleum-science



Original Paper

Adsorbed and free gas occurrence characteristics and controlling factors of deep shales in the southern Sichuan Basin, China



Shang-Wen Zhou a, b, Dong-Xiao Zhang a, c, *

- ^a Department of Energy and Resources Engineering, College of Engineering, Peking University, Beijing, 100871, China
- ^b PetroChina Research Institute of Petroleum Exploration and Development, Beijing, 100083, China
- ^c School of Environmental Science and Engineering, Southern University of Science and Technology, Shenzhen, Guangdong 518055, China

ARTICLE INFO

Article history: Received 22 August 2022 Received in revised form 15 October 2022 Accepted 11 December 2022 Available online 12 December 2022

Edited by Jie Hao and Teng Zhu

Keywords:
Adsorbed gas
Free gas
Gas occurrence characteristics
Deep shale

ABSTRACT

Deep shale gas (3500-4500 m) will be the important succeeding field for the growth of shale gas production in China. Under the condition of high temperature and high pressure in deep shale gas reservoirs, its gas occurrence characteristics are markedly different from those of medium and shallow layers. To elucidate the gas occurrence characteristics and controlling factors of deep shales in the Wufeng-Longmaxi Formation, methane adsorption, low-temperature N2, and CO2 adsorption experiments were conducted. The results show that in deep shales, the mesopores provide approximately 75% of the total specific surface area (SSA) and 90% of the total pore volume (PV). Based on two hypotheses and comparing the theoretical and actual adsorption capacity, it is speculated that methane is adsorbed in deep shale in the form of micropore filling, and free gas is mainly stored in the mesopores. Correlation analysis demonstrated that TOC is the key material constraint for the adsorption capacity of deep shale, and micropore SSA is the key spatial constraint. Other minerals and mesopore parameters have limited effect on the amount of adsorbed gas. Moreover, the free gas content ranges from 2.72 m³/t to 6.20 m³/t, with an average value of 4.60 m³/t, and the free gas content ratio is approximately 58%, suggesting that the deep shale gas reservoirs are dominated by free gas. This ratio may also increase to approximately 70% when considering the formation temperature effect on adsorbed gas. Gas density, porosity, and gas saturation are the main controlling factors of free gas content, resulting in significantly larger free gas content in deep shale than in shallower formations.

© 2022 The Authors. Publishing services by Elsevier B.V. on behalf of KeAi Communications Co. Ltd. This is an open access article under the CC BY-NC-ND license (http://creativecommons.org/licenses/by-nc-nd/4.0/).

1. Introduction

As an important natural gas resource and clean energy, the effective development of marine shale gas has been realized in China (Gong et al., 2020; Zou et al., 2021). In 2021, China's shale gas production increased significantly, reaching 22.8 billion cubic meters (Zou et al., 2022), which is primarily produced from layers shallower than 3500 m in the Sichuan Basin. The amount of shale gas resources in the southern Sichuan Basin exceeds 10 trillion cubic meters, of which deep resources contribute over 8 trillion cubic meters, accounting for over 80% (Ma et al., 2021; Zhang et al., 2022). The deep shale gas with a burial depth of 3500–4500 m will become an essential substitute for future production increases (Cai

* Corresponding author.

E-mail address: dxz@pku.edu.cn (D.-X. Zhang).

et al., 2021). In order to determine its basic geological properties and formulate appropriate development strategies, it is critical to elucidate the key characteristics of deep shale gas reservoirs.

Since there are three occurrence states of shale gas, i.e., adsorbed gas, free gas and dissolved gas, their quantities need to be summed when calculating geological reserves. Therefore, identifying the gas occurrence characteristics and their contents in shale is of great significance for in-depth understanding and evaluation of shale gas reservoirs (Ma et al., 2018; Li et al., 2019). Different from sandstone and carbonate gas reservoirs, adsorbed gas in shale can account for 20%–70% of the total gas content (Curtis, 2002). Thus far, the adsorption characteristics of shale and its controlling factors have been extensively studied, and the following findings have been demonstrated: (I) shale gas adsorption belongs to supercritical adsorption, and its isothermal adsorption curves will have a maximum value generally when the pressure is approximately 10 MPa, which is caused by the different increasing trends of

adsorbed-phase and gas-phase density with increasing pressure (Zhou et al., 2018). The absolute adsorption capacity should be transformed from excess adsorption capacity when evaluating its actual adsorption quantity, which will reach saturation under high pressure. (II) Shale gas adsorption belongs to a physical and exothermic process. Methane is generally adsorbed on the pore surface in the form of surface coverage or micropore-filling under the force of the pore wall (Zhou et al., 2018; Feng et al., 2020). In addition, affected by the adsorption force, methane molecules are preferentially adsorbed in the micropores under a certain pressure, leading the micropores to be the main storage space for the adsorbed gas (Mosher et al., 2013).

Furthermore, by combining the mineral content and pore structure parameters of shale, previous investigations have demonstrated that many factors can affect the adsorption capacity of shales (Fatah et al., 2020; Memon et al., 2020). Through a large number of experiments and correlation analyses, it has been confirmed that the content of organic matter and clay minerals are the material factors affecting the adsorption capacity of shale. In addition, specific surface area (SSA) is the internal factor, and moisture, temperature, and pressure are the external factors (Chen et al., 2016; Wang et al., 2016). Therefore, the adsorption capacity of shale under burial conditions is the comprehensive response to all of these factors. Compared with the medium-shallow shale that is already under industrial development, deep shale features higher formation temperature and pressure. In the Lu203 block of the southern Sichuan Basin, the average formation temperature and pressure can reach 130 °C and 80 MPa, respectively (Sun et al., 2022), causing its adsorbed and free gas occurrence characteristics to be quite different; however, this has rarely been studied. As a consequence, it is critical to investigate the gas adsorption mechanisms and characteristics of deep shales.

Free gas is the main phase of shale gas currently developed in China, and its content has a great impact on the initial production of shale gas wells. It is generally believed that the marine shale gas reservoirs developed in China are dominated by free gas, resulting in high initial production and rapid decline rate. For example, the test production of Well Lu203 can reach 1 million m³/d, but its decline rate can reach 70% within one year (Gou and Xu, 2019). The amount of free gas in shale cannot be directly tested, because a large amount of gas has been lost during drilling and coring, and thus it can only be recovered and calculated by mathematical models, such as USBM and the binomial method (Smith and Williams, 1984; Yee et al., 1993). However, the calculation results are frequently disputed because the different models can generate varied results. This is mainly because the coring time of shale gas wells is generally long, leading to a large loss of natural gas (Hao et al., 2013). Therefore, it is challenging to determine the free gas content in shale by the method of calculating lost gas during coring. Some researchers, however, have developed new experimental methods to test the free gas content in shale. For instance, O'Neill et al. (2021) proposed to use nuclear magnetic resonance (NMR) to measure adsorbed gas and free gas by collecting T_2 spectra of methane in coal and shale under different pressures. Li et al. (2022) adopted pressure-holding coring technology and carried out desorption metering to determine the free gas volume under the pressure dropping process, which constitutes a relatively direct and accurate method.

Since free gas is mainly stored in the pore space, its volume can also be calculated directly through the conventional calculation method on the basis of accurate determination of rock porosity (φ) and gas saturation (S_g) . When converting the gas volume to the standard state, it is also necessary to use the parameter gas volume coefficient (B_{gi}) or compressibility factor (Z), which are related to the formation temperature and pressure. Therefore, the calculated

free gas content is primarily affected by rock porosity, gas saturation, formation temperature, and pressure. Since these parameters will be markedly dissimilar for shale gas formations in different areas with various depths, the free gas volume will also be greatly different. However, for deep shale with very high temperature and pressure, whether the free gas volume increases or decreases is unclear, and relevant in-depth research is needed.

The purpose of this study is to elucidate adsorbed and free gas occurrence characteristics, mechanisms, and controlling factors in deep shales by multiple experiments and modeling analysis. Moreover, the variation law of adsorbed gas and free gas is clarified, and the root cause of high gas content in deep shale is identified. The results will provide useful guidance for evaluating the gasbearing capability of deep shale gas reservoirs in China.

2. Material and method

2.1. Geological background

Core samples were selected from two deep shale gas evaluation wells with a depth of approximately 4000 m in the Luzhou block in the southern Sichuan Basin, China. Black shale is widely developed in the Wufeng-Longmaxi Formations (O_3w-S_1l) in southern China (Fig. 1a), and the ages belong to the Late Ordovician Kediian, Hernantian, and the Early Silurian Rudanian, Eronian, and Trechiian. The Wufeng Formation and Longmaxi Formation belong to continuous sedimentation, and thus they exhibit conformity contact. The lower part of the Longmaxi Formation shale is mainly black, gray-black thin-layered shale or massive shale with well-developed bedding, while the upper part is gray-green, yellow-green shale and sandy shale, sometimes with siltstone or argillaceous limestone (Xu et al., 2019).

According to lithological and electrical characteristics, the lower part of the Longmaxi Formation can be divided into four sublayers: $S_1l_1^1$; $S_1l_1^2$; $S_1l_1^2$; and $S_1l_1^4$ (Fig. 1b). For the selected samples, the organic maturity (R_0) is 2.14%–2.56%, with an average of 2.33%, indicating that it is in the over-mature stage, and the main gas product is dry gas generated from the cracking of liquid hydrocarbon. The kerogen composition of all of the samples is dominated by sapropel, and its kerogen belongs to type I. Detailed basic information about these samples is presented in the Supplemental Material.

2.2. TOC and mineral composition analysis

TOC tests were conducted with an LECO CS-200 sulfur-carbon analyzer. Prior to the experiment, the inorganic content in the samples was removed with hydrochloric acid. The TOC content was calculated by CO₂ content produced by complete combustion of the high temperature combustion method (Tang et al., 2014). XRD experiments were performed with an X-ray diffractometer at the rotation angle of 3°-45°, tube pressure of 45 kV, and current of 100 mA. Quantitative analysis adopted the step-scan method with a scanning speed of 4°/min and a sampling interval of 0.02°. The nonclay mineral content was calculated by the K value method of diffraction spectra of conventional glass slides, and the relative content of clay minerals was determined by the N/E/T glass slide (The glass slides in three different stages are respectively natural orientation glass slides/ethylene glycol saturated glass slides/high temperature glass slides) diffraction peak area subtraction method (Ward, 2016).

2.3. Low temperature and pressure N_2/CO_2 adsorption test

Low temperature and pressure N₂/CO₂ adsorption tests were

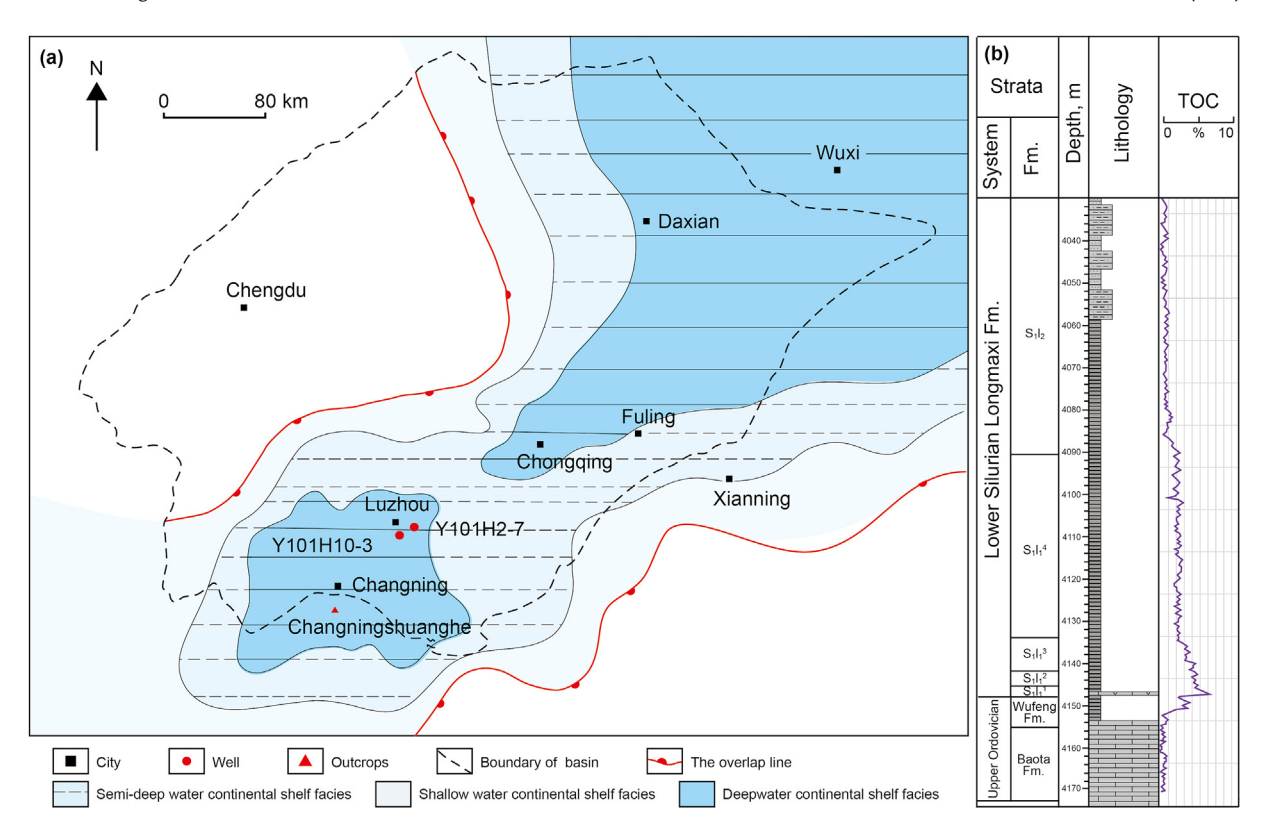


Fig. 1. The deep shale gas well sites, geographical locations (a), and single-well histogram (b).

conducted with the same instrument, i.e., the Micromeritics ASAP 2420 automatic specific surface area and pore analyzer. At the experimental temperature of $-196\,^{\circ}\text{C}$, the relative pressure of the low-temperature N2 adsorption test was $p/p_0=0.0095-0.995$. The mesopore specific surface area (SSA) was calculated by the BET equation (Brunauer et al., 1938; Wang et al., 2018; Zhou et al., 2019). The low temperature CO2 adsorption experiment was performed at 0 °C. Given the high saturated vapor pressure of CO2 (3.48 MPa), the CO2 adsorption-desorption isotherm could only be tested within $p/p_0=0.00001-0.03$. The micropore SSA can be calculated by the Dubinin–Radushkevich (DR) equation (Dubinin and Astakhov, 1971; Huston and Yang, 1997; Sakurovs et al., 2007) based on micropore-filling theory.

2.4. Methane adsorption experiments

Isothermal methane adsorption experiments of the deep shales were conducted by a gravimetric adsorption analyzer, featuring a magnetic suspension balance (MSB) with a high weight accuracy of 10 μg (Sakurovs et al., 2007). Its maximum test temperature and pressure can reach 150 °C and 35 MPa, respectively. The experimental temperature and pressure were set as 60 °C and 20 MPa, respectively, in this study to ensure data stability. At constant temperature, methane was adsorbed under different pressure levels, and formed an inherent adsorbed phase over the surface of shale. The reading of the balance is the joint result of the gravity and buoyancy of the sample, barrel, and adsorbed phase. When considering the existence of the adsorbed-phase volume, instead of directly measuring the actual adsorption capacity (i.e., the absolute adsorption capacity), the isothermal adsorption experiment can measure the excess adsorption capacity (V_{ex}) (Do and Do, 2003; Klewiah et al., 2020).

$$m_{\rm ex} = \Delta m - m_{\rm sc} - m_{\rm s} + (V_{\rm sc} + V_{\rm s}) \times \rho_{\rm g} \tag{1}$$

$$V_{\rm ex} = \frac{m_{\rm ex} \times 22.4 \times 1000}{m_{\rm s} \times 16} \tag{2}$$

where $m_{\rm ex}$ is the excess adsorption capacity of methane, g; $V_{\rm ex}$ is the excess adsorption capacity of methane, m³/t; Δm is the reading of the magnetic suspension balance, g; $m_{\rm sc}$ is the mass of the sample barrel, g; $m_{\rm s}$ is the mass of the sample, g; $V_{\rm sc}$ is the volume of the sample barrel, cm³; $V_{\rm s}$ is the volume of the sample, cm³; $\rho_{\rm g}$ is the density of the methane gas at different pressure points, g/cm³; and $\rho_{\rm a}$ is the density of the adsorbed methane, g/cm³.

To describe the adsorption behaviors and characteristics of methane in shale, the Langmuir adsorption model is commonly used in previous studies, and it achieves a good application effect. In this study, the Langmuir-based excess adsorption model was used to fit the isothermal adsorption curves and determine the maximum adsorption capacity of the shale samples.

$$V_{\rm ex} = \frac{V_{\rm L}P}{P_{\rm L} + P} \left(1 - \frac{\rho_{\rm g}}{\rho_{\rm a}} \right) \tag{3}$$

where $V_{\rm ex}$ is the tested adsorption quantity, ${\rm m^3/t}$; P is the test equilibrium pressure, MPa; $V_{\rm L}$ is the maximum saturated adsorption quantity (Langmuir volume), ${\rm m^3/t}$; and $P_{\rm L}$ is the Langmuir pressure, MPa.

3. Results

3.1. Mineral composition

The mineral composition of the marine deep shales is primarily

composed of quartz and clay minerals, and they account for approximately 42.2% and 25.5% of the total mineral contents, respectively (Fig. 2). In addition, some plagioclase, calcite, dolomite, and pyrite are also detected. Obviously, the content of quartz increases with increasing depth, while that of clay minerals is the opposite. In the Wufeng Formation, the quartz content begins to decrease, while the clay mineral content begins to increase. According to the "high elastic modulus, low Poisson ratio criterion", quartz, dolomite, and pyrite were considered as high brittleness minerals (Grieser and Bray, 2007). In this sense, the calculated shale brittleness index is 40.7%—76.8%. It also increased with depth, reaching its maximum value at the bottom layer of the Longmaxi Formation.

Regarding the clay mineral composition, these deep shale samples mainly contain illite, chlorite, and illite/smectite mixed

layer, which is a typical clay mineral composition structure of marine shales. Among them, the content of illite is the highest, with a mean value of 60.9% of total clay minerals. The types and contents of clay minerals possess certain guiding significance about the deposition environment and evolution sequence of shale layers (Chen et al., 2020). The tested clay mineral composition of the deep shale shows that it was deposited in a semiarid-arid paleoclimate, and the water was alkalescent and rich in K⁺, in its diagenetic period. It is indicated that the deep shales reached the late diagenetic evolution stage, and hydrocarbons evolved into the dry gas stage, showing that they are available for the formation of shale gas under extensive gas source conditions. There is little difference in mineral composition and brittleness index between deep shale and medium-shallow shale, and both identify the bottom of the Longmaxi Formation as the engineering sweet spot. However, further

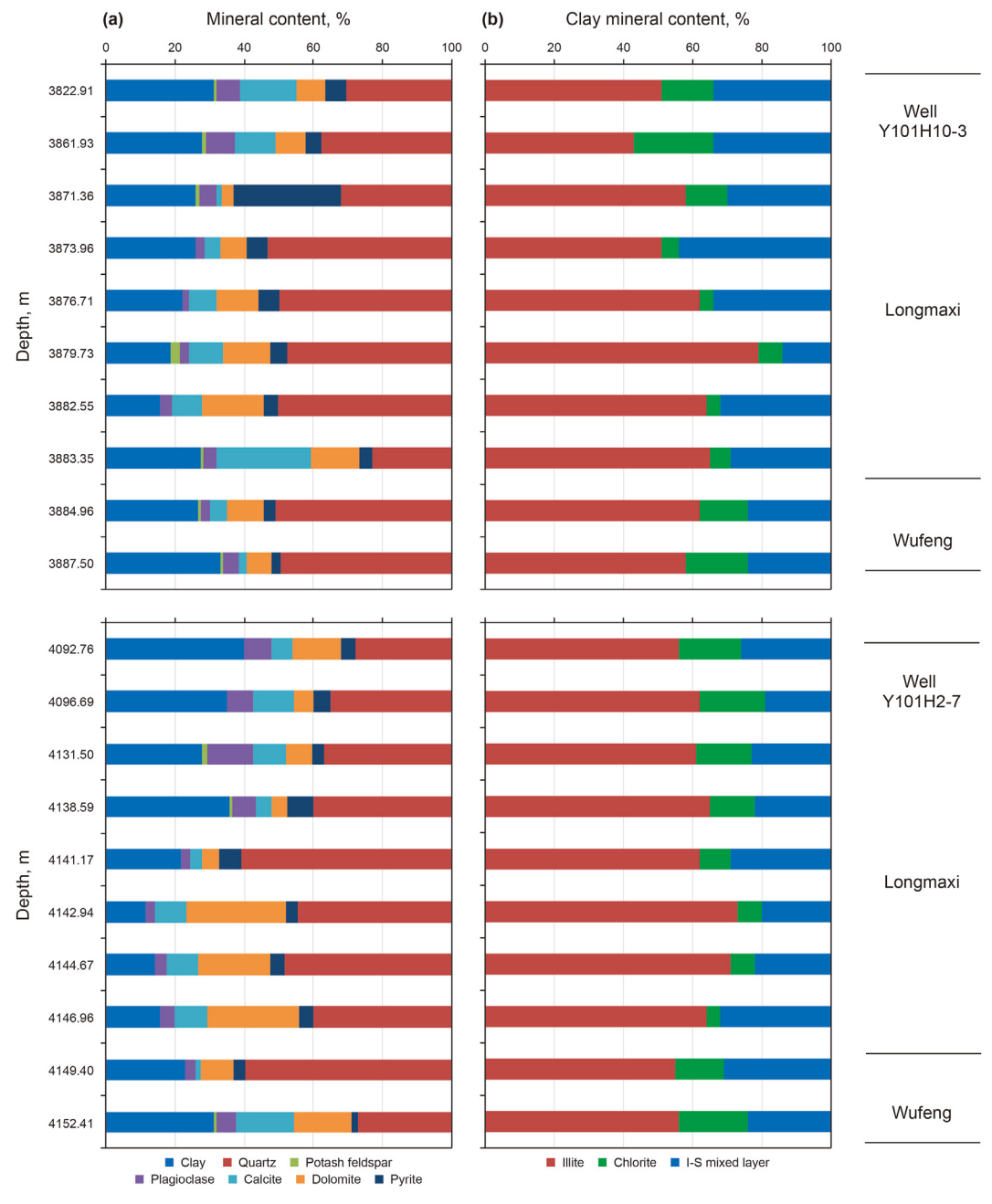


Fig. 2. Variation of whole rock mineral (a) and clay mineral (b) content of the deep shale samples with depth.

comparison demonstrated that the calcite content of deep shales is relatively lower. In the studied two deep shale wells, the average calcite content is only 8.8%, compared to approximately 20% for the medium-shallow shale in the southern Sichuan Basin (Singh et al., 2009; Ma et al., 2022).

3.2. SSA and PV results

The low temperature and pressure N_2 adsorption curves of the representative samples shown in Fig. 3 are all S-shaped and are typical type IV isotherms (Jiao et al., 2021). According to the shape of hysteresis loops, all of the curves can be deemed to be H3 type, reflecting the relative development of mesopores. A sudden evaporation phenomenon occurs when $p/p_0=0.45$, suggesting the existence of fine bottleneck or ink bottle pores inside the shale (Liu et al., 2018). The adsorption branch exhibited obvious capillary condensation around $p/p_0=0.9$, resulting in a sharp increase in adsorption capacity, but not saturation, indicating that all shale samples developed micro-fractures or parallel-plate pores.

Unlike the N_2 adsorption curve, the low temperature CO_2 adsorption curve tends towards a type I isotherm. Although both are subcritical adsorption, the test pressure range is different. Because the experimental temperature is far from reaching the CO_2 saturated vapor pressure, the upward trend of its adsorption curve is still obvious. Furthermore, there is no steep rising phase, as the partial pressure (p/p_0) required for capillary condensation cannot be reached. Moreover, the kinetics of CO_2 molecules are sufficient to enter smaller pores at 0 °C than N_2 molecules at -196 °C. For this reason, we always use N_2 adsorption to analyze the SSA and pore size distribution (PSD) of mesopores (2–50 nm) and CO_2 adsorption to analyze the SSA and PSD of micropores (0–2 nm).

For all of the deep shale samples, as shown in Fig. 4, the mesopore SSA is $17.70-32.77 \text{ m}^2/\text{g}$ with an average of $24.76 \text{ m}^2/\text{g}$; the mesopore volume (PV) is $0.0239-0.0450 \text{ cm}^3/\text{g}$ with an average of

 $0.0345~{\rm cm^3/g}$. The micropore SSA is $6.41-11.60~{\rm m^2/g}$ with a mean value of $9.05~{\rm m^2/g}$; the micropore volume (PV) is $0.00217-0.00399~{\rm cm^3/g}$ with a mean value of $0.00303~{\rm cm^3/g}$. Overall, the micropore PV accounts for less than 10% of the total PV, and the micropore SSA accounts for approximately 25% of the total SSA. This suggests that, for marine deep shale, mesopores provide the main reservoir spaces for gas storage; whereas, micropores can only provide limited surface area for adsorbed gas.

3.3. Methane adsorption isotherms

The isothermal adsorption curves of the deep shales are shown in Fig. 5. As the pressure increases, the adsorption capacity first increases and then decreases, reaching its maximum at approximately 10 MPa in almost all cases. The adsorption data are presented in the Supplemental Material. With pressure increasing, the adsorbed-phase density increases first and then reaches stability, while the gas-phase density increases continuously. Therefore, the density difference between the two will reach a maximum value. After that, this difference will begin to reduce, as represented by the decline trend of the adsorption curve. Essentially, this is associated with the pore structure features within the sample itself. Different samples possess different pore development characteristics and different adsorption capacities, which eventually account for the different trends of the descending part of the curves.

For deep shale, to obtain the true adsorption capacity, the experimental pressure and temperature (P and T) need to be set to approximately 80 MPa and 130 °C, respectively. Unfortunately, most of the currently available experimental systems cannot provide these P/T conditions. Since the experimental system used in this paper was unable to provide the requisite formation P/T conditions, only the adsorption curves yielded under experimental P/T (20 MPa and 60 °C) can be used to predict the adsorption capacity under formation P/T conditions (Zhou et al., 2022). As the pressure

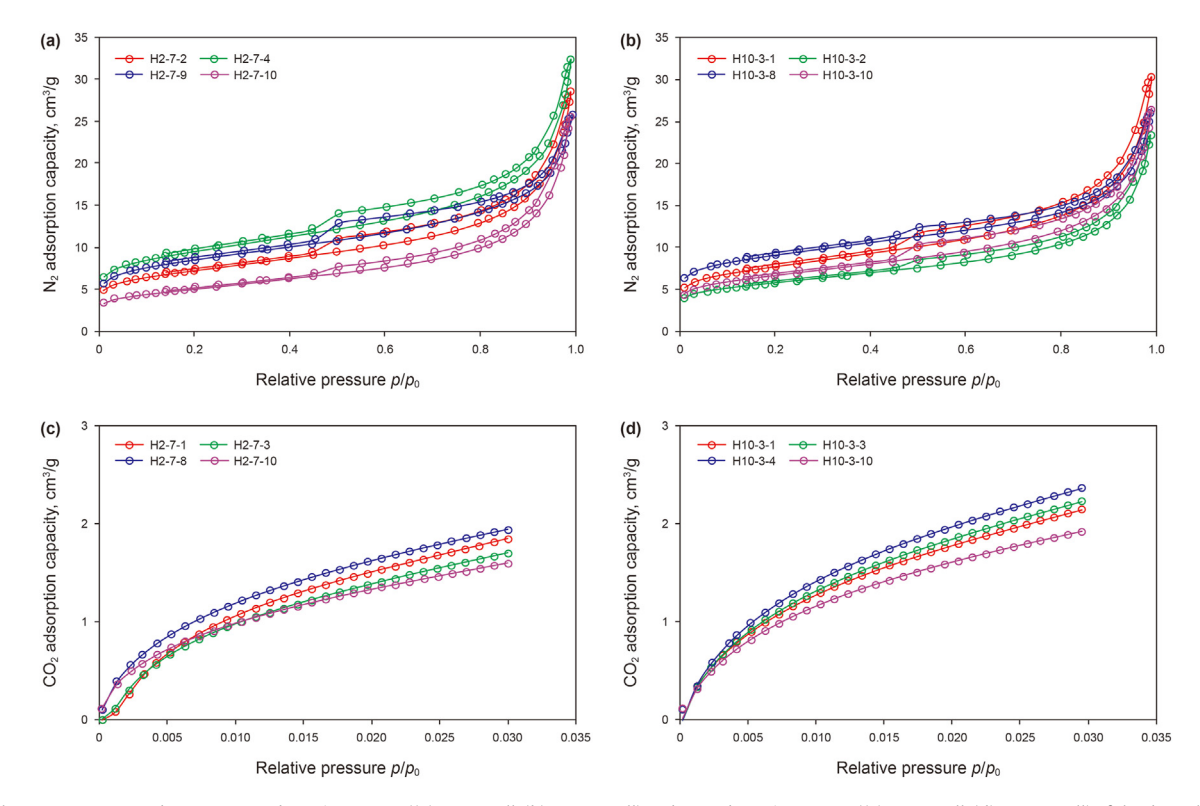


Fig. 3. The low temperature and pressure N2 adsorption curves ((a) H2-7 well, (b) H10-3 well) and CO2 adsorption curves ((c) H2-7 well, (d) H10-3 well) of the deep shale samples.

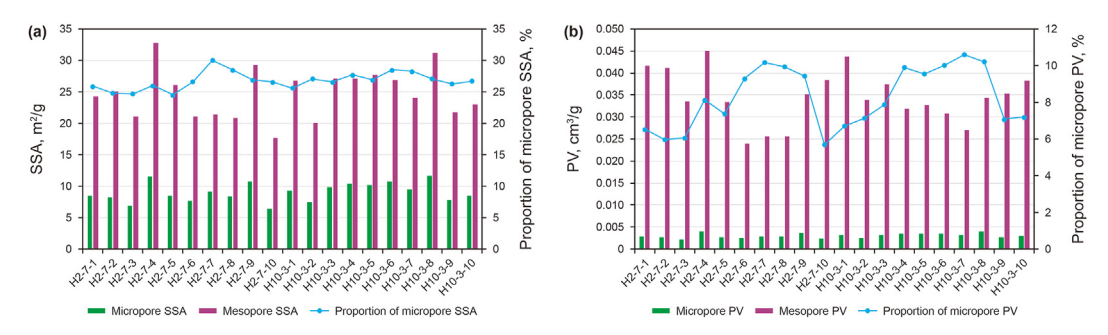


Fig. 4. The specific surface area (SSA) (a) and pore volume (PV) (b) of the micropores and mesopores based on the low temperature and pressure N₂/CO₂ adsorption tests.

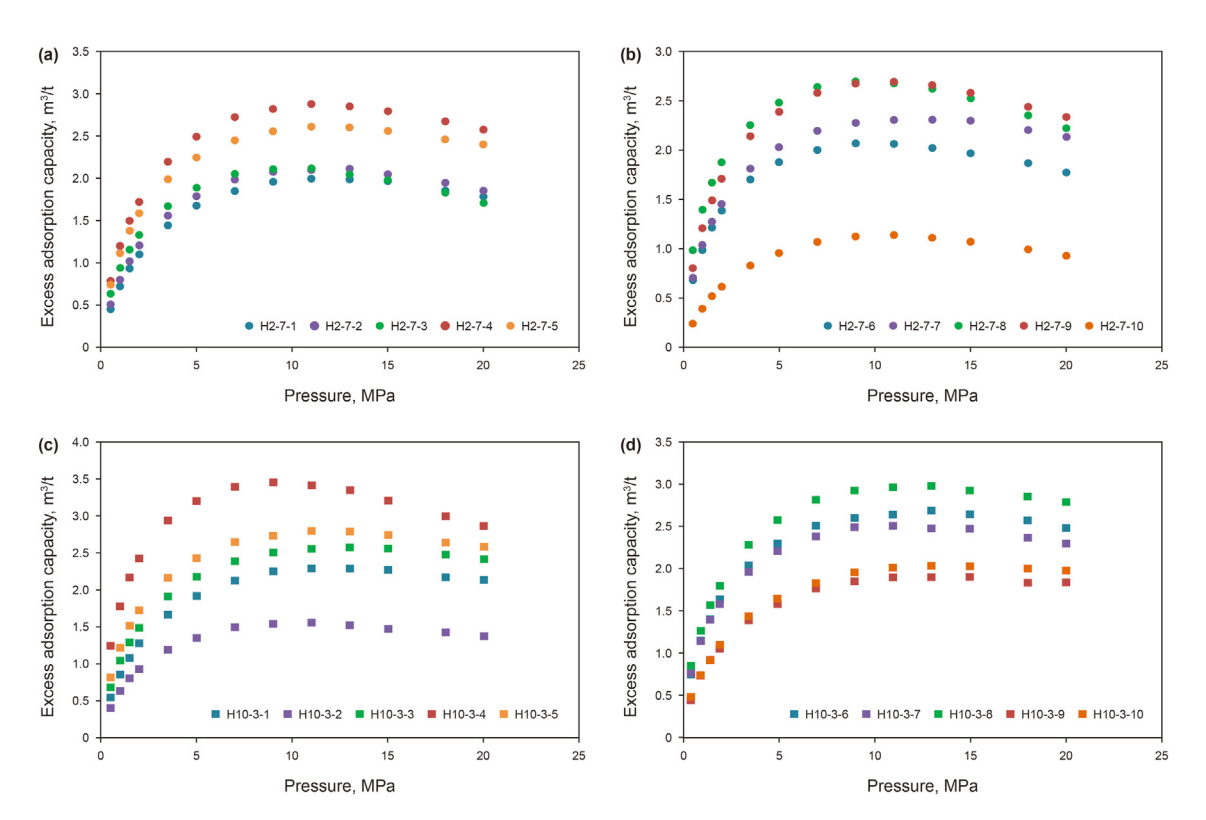


Fig. 5. Methane isothermal adsorption curves of deep shale samples at 60 °C and 20 MPa ((a, b) Well H2-7, (c, d) Well H10-3).

further increases, the variation law of curves in the graphs will not change, except that the decline rate is slower. Under ultrahigh pressure conditions, the adsorbed gas capacity will reach saturation and be a maximum value (Langmuir volume). Consequently, to facilitate comparison, Langmuir volume (V_L) is used to represent the adsorbed gas content of the studied deep shale samples. It is worth noting that, affected by the high formation temperature, the actual adsorption amount will be lower than its Langmuir volume.

4. Discussion

4.1. Adsorbed gas occurrence characteristics

Combined with the results of microscopic pore structure analysis and isothermal adsorption test, the occurrence characteristics of adsorbed methane molecules were analyzed. If it is assumed that methane is mainly adsorbed in shale pores in the form of monolayer adsorption or micropore-filling, the theoretical monolayer-adsorbed amount can be calculated by the pore SSA or PV. By comparing the actual adsorption capacity with the theoretical

adsorption capacity (TAC), the assumption of monolayer or micropore-filling adsorption can be proven or disproven. The TAC based on monolayer adsorption theory can be calculated by the following equation (hypothesis I):

$$V_{\rm tm} = \frac{SSA}{A_{\rm m} \times N_{\rm a}} \times 22.4 \times 1000 \tag{4}$$

Similarly, the TAC based on micropore-filling theory can be calculated by the following equation (hypothesis II):

$$V_{\rm tp} = \frac{PV}{V_{\rm m} \times N_{\rm a}} \times 22.4 \times 1000 \tag{5}$$

where $V_{\rm tm}$ is the monolayer theoretical adsorption capacity (TAC-ml), m³/t; $V_{\rm tp}$ is the micropore-filling theoretical adsorption capacity (TAC-mf), m³/t; SSA is the pore SSA, m²/g; PV is the pore volume, m³/g; $A_{\rm m}$ is the area occupied by a single methane molecule, approximately 1.134×10^{-19} m²; $V_{\rm m}$ is the volume occupied by a single methane molecule, approximately 2.873×10^{-29} m³; and $V_{\rm m}$ is the Avogadro's constant number, with a value of 6.02×10^{23} .

When we use the micropore or mesopore SSA in Eq. (2), the TAC-ml of micropores and mesopores can be obtained, as shown in Fig. 6a. Moreover, when we use the micropore or mesopore PV in Eq. (3), the TAC-mf of micropores and mesopores can be obtained, as shown in Fig. 6b.

For hypothesis I, from Fig. 6a, it can be seen that the micropore TAC is only slightly lower than the Langmuir volume, while the Langmuir volume is much lower than the mesopore TAC. This indicates that the micropores developed in deep shales can provide most of the surface area for the monolayer adsorption of methane molecules, and only a few surface areas need to be provided by mesopores. For hypothesis II, from Fig. 6b, it can be seen that the micropore TAC is slightly higher than the Langmuir volume, while the Langmuir volume is significantly lower than the mesopore TAC. This suggests that the micropores developed in deep shales can provide all of the spaces for the filling of methane molecules, and mesopores are not required to provide pore space for adsorption.

According to the adsorption potential theory, the adsorption potential on the solid surface is mainly controlled by its curvature. Among the pores in the three pore size ranges of micropore, mesopore and macropore, the curvature of the micropore wall is the largest, and thus the surface of the micropores has a higher adsorption potential and can preferentially adsorb methane molecules (Huang et al., 2020). As a consequence, when the adsorption space is sufficient, the gas molecules will be preferentially adsorbed in the micropores in the form of filling, as shown in Fig. 6b. In summary, the occurrence characteristics of adsorbed gas in deep marine shales is that all of the methane molecules are adsorbed in the micropores in the form of micropore-filling, and no methane molecules are adsorbed in the mesopores. Therefore, overall, hypothesis II is more reasonable.

For different types of shale gas reservoirs, their developed pore structures are dissimilar, which may lead to different adsorption mechanisms. For the Silurian marine shale discussed in this study, due to the development of a certain proportion of micropores, although its volume is much smaller than that of mesopores, the

above hypothesis also proves that it is sufficient to contain and adsorb methane molecules. For continental shale with relatively less-developed pores, its adsorption mechanism may be different. Based on the above assumptions, when the micropore volume is insufficient to fill enough methane molecules, some molecules will be stored in the mesopore in the form of monolayer adsorption.

4.2. Free gas occurrence characteristics

Different from adsorbed gas, free gas mainly exists in the inner space of pores in a free state, and the greater is the porosity, the larger is the amount of free gas. Under standard conditions, the amount of free gas in shale can be calculated by the following equations (Huang et al., 2020):

$$V_{\rm f} = \rho_{\rm g} \times \varphi \times 22.4 \times 1000 \times S_{\rm g} / 16 / \rho_{\rm s}$$
 (6)

$$V_{\rm f} = \varphi \times S_{\rm g} / B_{\rm gi} / \rho_{\rm s} \tag{7}$$

$$B_{gi} = Zp_{sc}T_i/(p_iT_{sc}) \tag{8}$$

where V_f is the free gas content, m³/t; ρ_g is the bulk gas density, g/cm³; φ is the core porosity, %; S_g is the gas saturation, %; ρ_s is the rock density, g/cm³; B_{gi} is the gas volume coefficient; Z is the compression factor of methane; p_{sc} is the standard pressure, 0.1 MPa; T_{sc} is the standard temperature, 293.15 K; and p_i and T_i are the formation pressure and temperature, respectively.

For the deep Longmaxi shales in this study, their formation pressure and temperature are approximately 80 MPa and 130 °C, respectively, yielding a methane density of approximately 0.26 g/cm³. In addition, the average gas saturation of the Longmaxi shales is approximately 70%, the mean rock density is approximately 2.59 g/cm³, and the porosity ranges from 2.83% to 6.33%. Therefore, the free gas content calculated by Eq. (3) ranges from 2.72 m³/t to

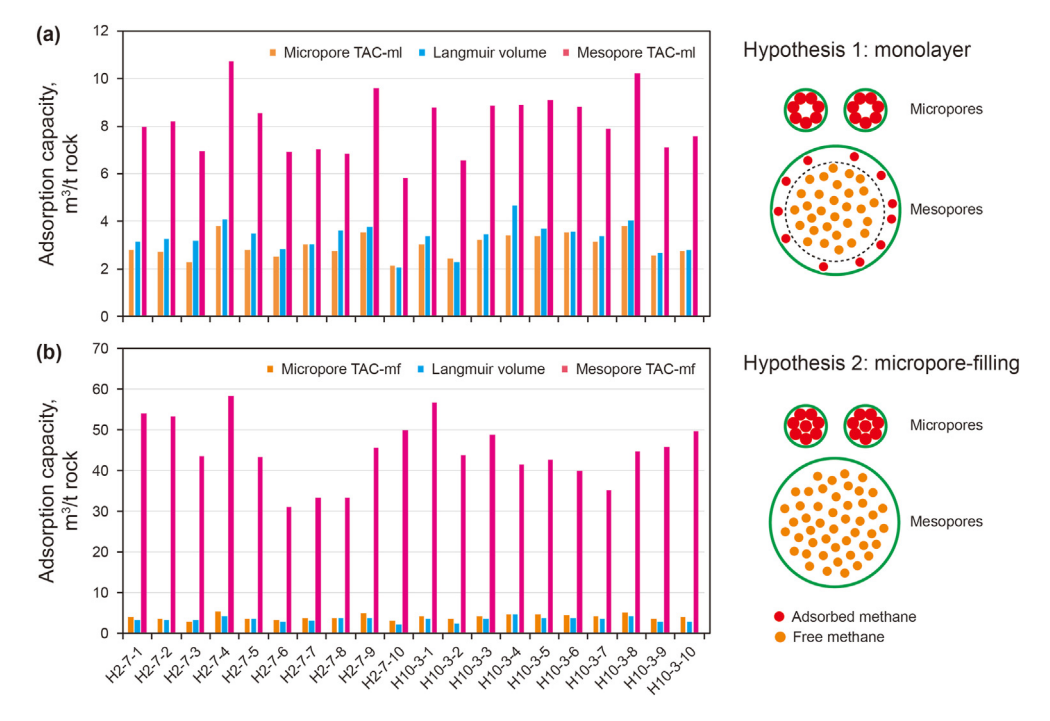


Fig. 6. The comparison among the microporous TAC, mesoporous TAC and Langmuir volumes based on monolayer adsorption theory (a) and microporous filling theory (b), respectively, and the schematic diagram of adsorbed and free gas occurrence state based on the two hypotheses.

6.20 m³/t, with an average value of 4.60 m³/t. It can be seen that the free gas content is larger than the adsorbed gas content, and this is mainly due to the relatively large porosity and gas saturation in the studied deep shales. In particular, since the free gas is mainly stored in the mesopores, when the mesopore volume is large, the free gas volume will also be relatively high.

Without considering the dissolved gas in shale, the total gas content can be obtained by adding the adsorbed gas and free gas content, as shown in Fig. 7. It can be seen that the total gas content is between 5.01 m³/t and 10.25 m³/t, with an average of 7.91 m³/t. Moreover, the proportion of free gas content is approximately 58%. It should be noted that the adsorption capacity discussed above is obtained at the experimental temperature (60 °C). Under actual formation conditions (130 °C), however, the adsorbed gas volume will be reduced by approximately 20% (Zhang et al., 2012; Mosher et al., 2013; Merey and Sinayuc, 2018; Zou et al., 2019; Zhou et al., 2022). Therefore, the adsorbed gas ratio will decrease, and the free gas ratio will increase to approximately 70%. This suggests that the deep shale gas reservoirs are dominated by free gas, and a high proportion of free gas means that the initial production of shale gas wells will be larger.

4.3. Controlling factors of adsorbed gas

For the controlling factors of adsorbed gas volume, our analysis proceeds from two aspects: pore structure and mineral composition. The correlation analysis results are presented in Fig. 8. It can be seen that TOC is well correlated with adsorption capacity; whereas, the content of quartz, clays, and illite have a poor correlation with adsorption capacity. This reveals that, in terms of mineral composition, organic matter (OM) is the most critical material constraint for adsorbed gas content in deep shales. Clay minerals have little control over their adsorption capacity, although clays are a good adsorbent and are strongly adsorptive to gases. Regarding mediumshallow marine and continental shale, many studies have reported that clay mineral content, to some extent, controls the adsorbed gas content of shale (Gasparik et al., 2013; Zhu et al., 2020; Jiang et al., 2021). However, another important feature of clay minerals is their strong water adsorptivity and high water saturation in shale. As water can occupy the adsorption site of clay minerals, the adsorptivity of clay minerals to methane in marine deep shales is diminished (Chen et al., 2016; Saidian et al., 2016). In addition, as the

adsorptivity of organic matter to methane is significantly stronger than illite and other clay minerals, and due to the commonly high organic content in marine Longmaxi Formation shale, the adsorptivity of OM to methane is much greater than the weak adsorptivity of clay minerals to methane.

The correlation between gas adsorption capacity and pore structure parameters is shown in Fig. 8e and f. Gas adsorption capacity is better correlated with SSA than PV, which is in accordance with the basic principle of gas adsorption theory. Regardless of micropore or mesopores, SSA is well correlated with gas adsorption capacity, and micropore SSA has a higher correlation. In terms of the controlling role of pore volume, mesopore volume is not significantly correlated with gas adsorption capacity, while micropore volume is well correlated. Overall, micropores in deep shales are the main reservoir spaces for adsorbed gas. This is consistent with the adsorbed gas occurrence characteristics analyzed in Section 4.1. Through comparison, it is found that the shale samples in this reference were taken from geological shallow wells, and the measured total pore volume is only approximately 0.005 cm³/g, while the pore volume of the samples taken in this study is much larger than this value, which can reach approximately 0.04 cm³/g. This shows that under the same experimental method, the pores of the samples taken in the literature were not developed, which may be an important reason for the negative correlation between the micropore volume and the adsorption capacity.

4.4. Controlling factors of free gas

From Eq. (3), the controlling factors of free gas volume can be obtained more directly. Obviously, it is primarily controlled by three key parameters: gas density; porosity; and gas saturation. Among them, gas density is correlated with formation pressure and temperature. As the depth increases, the formation temperature and pressure will increase, but the influence trend of pressure and temperature on methane gas density is opposite. With the increase of formation pressure, the gas density increases, while the gas density decreases with the increase of formation temperature. Affected by these two key factors, the gas density will first increase rapidly and then increase slowly, as shown in Fig. 9. At the same time, the gas volume coefficient (B_{gi}) decreases with the increase of depth; whereas, the compression factor (Z) decreases first and then increases with the increase of depth, and reaches a minimum value

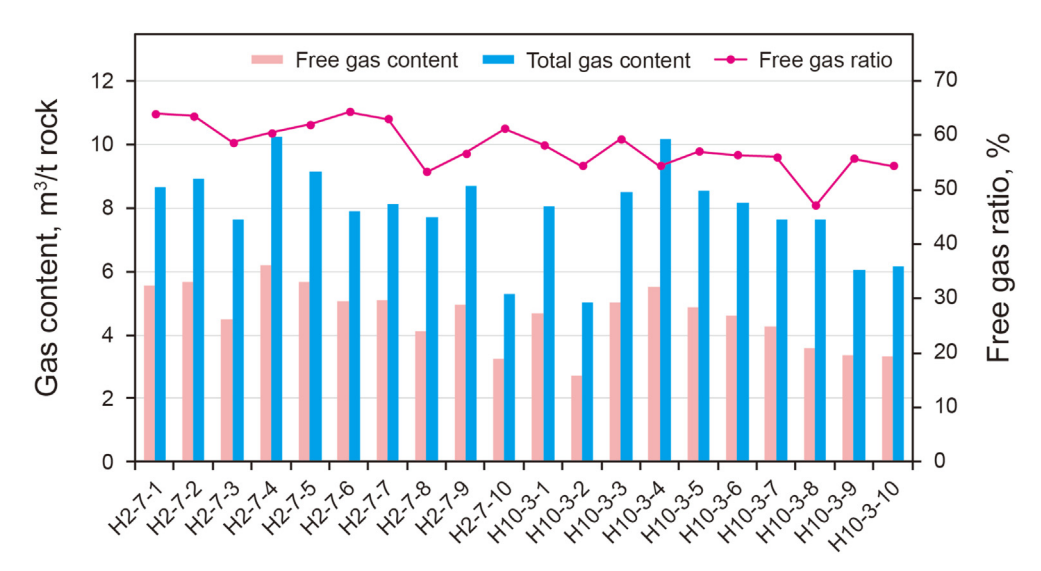


Fig. 7. The calculated free gas and total gas content, and free gas ratio of the total gas content.

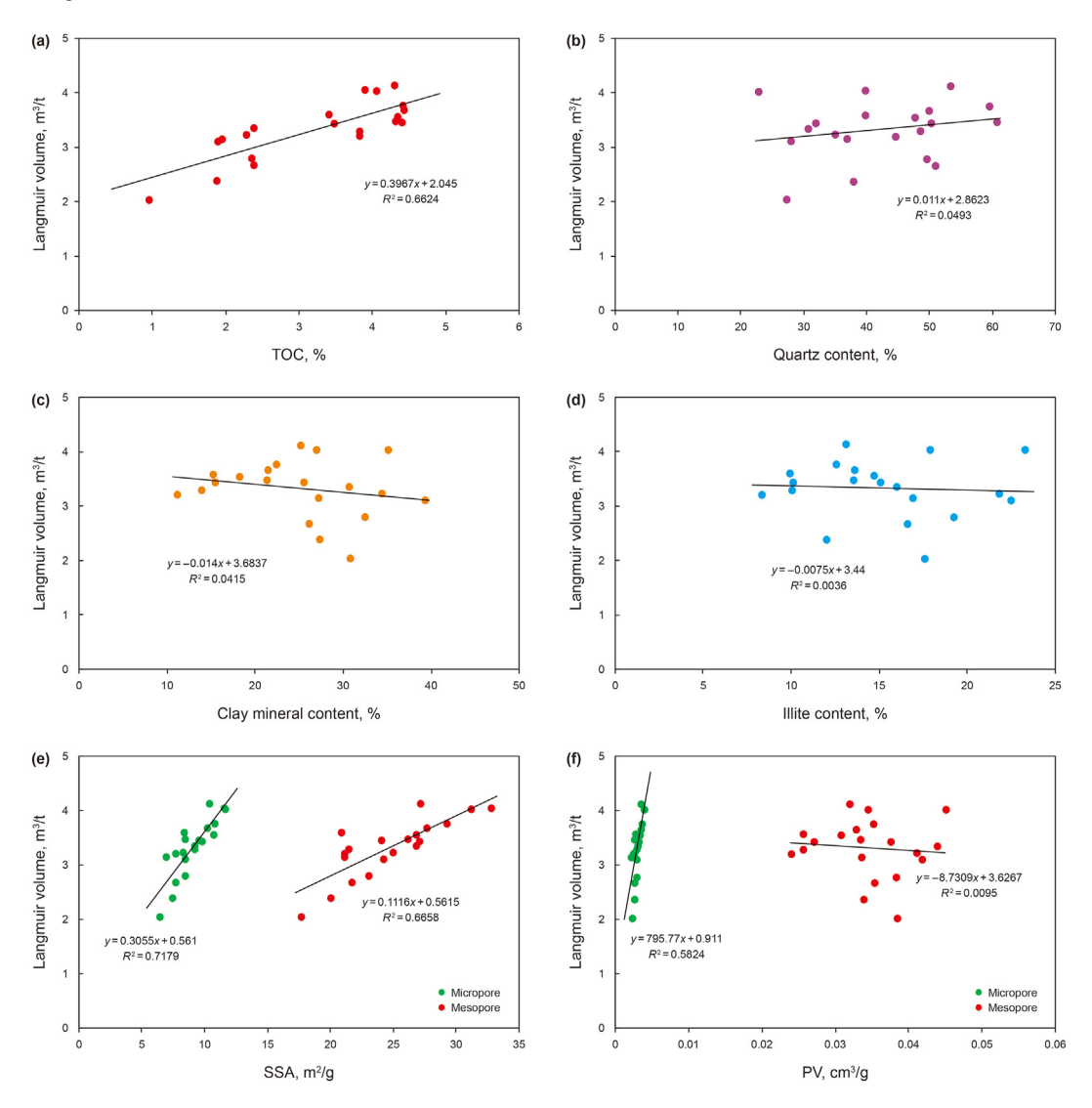


Fig. 8. Relationships between mineral composition ((a) TOC, (b) Quartz content, (c) Clay mineral content, (d) Illite content), pore structure parameters ((e) SSA, (f) PV), and methane adsorption capacity of the deep shale samples.

at the depth of approximately 1000 m. Overall, within the depth range of the deep shale gas reservoir (3500 m–4500 m), the gas density, compression factor, and volume coefficient have all been in a stage of slight change. However, compared with shallower layers, the changes of these parameters will lead to the increase of free gas content in deep shale. Moreover, when it is further increased to approximately 5000 m, the free gas content will not change significantly.

In addition, it is obvious that porosity and gas saturation control the free gas content. Porosity and gas saturation are inherent properties of reservoir rocks. When organic-rich shale has a strong gas-generating capacity, strong rock resistance to compaction, and good gas preservation conditions, under the combined action of these factors, its porosity and gas saturation will be higher. Generally, shales from the S1¹ sublayer have larger porosity and higher gas saturation than other sublayers, and thus the free gas content always reaches its highest value at the bottom of the Longmaxi Formation.

For deep shale gas reservoirs, the most important feature is that the formation temperature and pressure are very high. Affected by these conditions, the mineral composition, pore development characteristics, and gas occurrence state will all change. In this study, combining with the micro-pore structure, mineral composition and gas physical characteristics, the gas occurrence characteristics and its controlling factors of deep shales are analyzed, and some new understandings are obtained. It is worth noting that the influence of water content was not considered in the analysis of adsorbed gas content in this study. In fact, the water content in shale also has a certain influence on the gas occurrence state and capacity (Yang et al., 2017; Wang et al., 2020). Considering the influence of water content, the modes of gas occurrence discussed in this study may have some differences. Water molecules may preferentially occupy the adsorption sites of micropores, leading to the weakened gas adsorption. In follow-up work, we will discuss the gas occurrence characteristics under water-bearing conditions, and carry out an in-depth comparison of deep and shallow shale gas reservoirs.

5. Conclusions

To clarify the adsorbed and free gas occurrence characteristics and controlling factors of deep shales in China, multiple

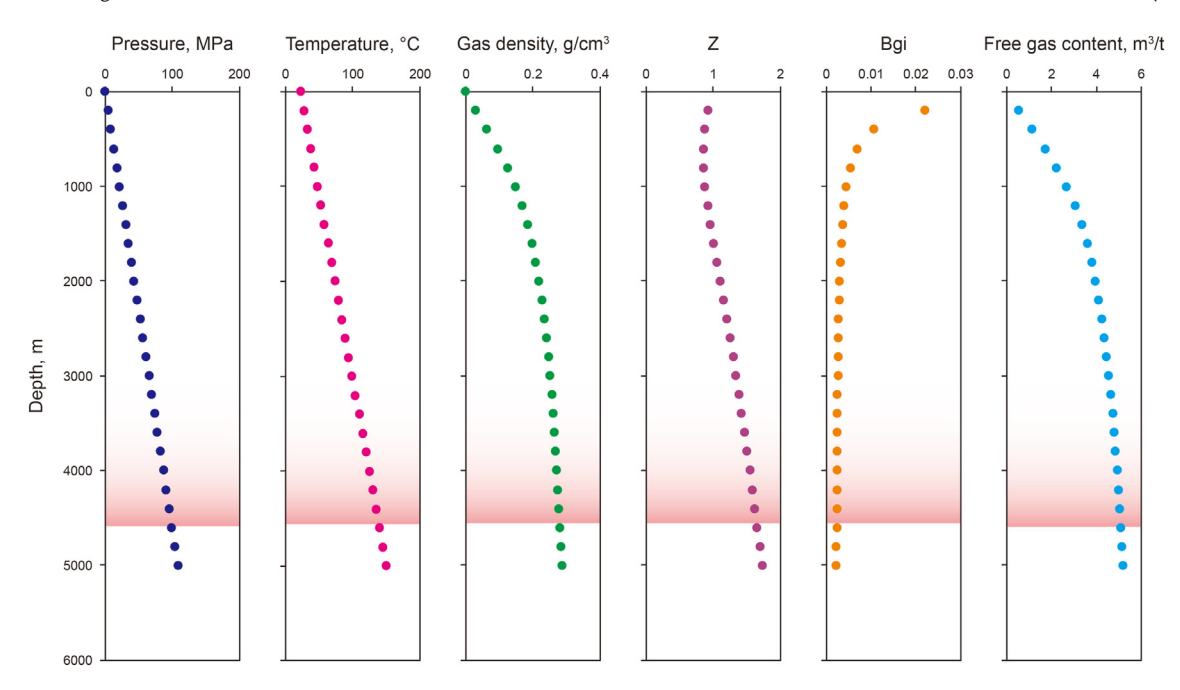


Fig. 9. Variation of formation pressure, temperature, gas density, compression factor, and volume coefficient with depth. The pressure gradient and temperature gradient are set to 2.16 MPa/100 m and 2.57 °C/100 m, according to the actual data of the deep shale gas field in the studied area.

experiments were performed on shale samples from the Wufeng-Longmaxi Formation. The main conclusions are as follows:

- (1) By comparing the theoretical and actual adsorption capacity, it is shown that micropores developed in deep shales can provide all of the spaces for the filling of methane molecules, and thus methane is preferentially and dominantly adsorbed in micropores in the form of pore-filling.
- (2) The free gas content ranges from 2.72 m³/t to 6.20 m³/t, with an average value of 4.60 m³/t, and the free gas volume ratio is approximately 58%, suggesting that the deep shale gas reservoirs are dominated by free gas. This ratio will increase to approximately 70% when considering the formation temperature effect on adsorbed gas.
- (3) TOC is the key material constraint for the adsorption capacity of deep shales, while micropore SSA is the key spatial constraint. Other minerals (quartz, clay, etc.) and mesopore parameters have limited effect on the amount of adsorbed gas.
- (4) Gas density, porosity, and gas saturation are the main controlling factors of free gas content, resulting in a significantly larger free gas content in deep shale than in shallower formations.

CRediT authorship contribution statement

Shang-Wen Zhou: methodology, validation, writing - original draft. **Dong-Xiao Zhang:** conceptualization, writing - review and editing.

Declaration of competing interest

The authors declare that they have no known competing financial interests or personal relationships that could have appeared to influence the work reported in this paper.

Acknowledgments

This study was funded by a PetroChina Basic Technology Research Project (No. 2021DJ1905).

Appendix A. Supplementary data

Supplementary data to this article can be found online at https://doi.org/10.1016/j.petsci.2022.12.006.

References

Brunauer, S., Emmett, P.H., Teller, E., 1938. Adsorption of gases in multimolecular layers. J. Am. Chem. Soc. 60 (2), 309–319. https://doi.org/10.1021/ja01269a023.

Cai, J.C., Tian, Z.H., Zhou, S.W., et al., 2021. Controlling factor analysis of microstructural property and storage capacity of deep Longmaxi Formation shale in Sichuan Basin. Energy Fuel. 35, 20092–20102. https://doi.org/10.1021/ acs.energyfuels.1c03495.

Chen, F.W., Zheng, Q., Ding, X., et al., 2020. Pore size distributions contributed by OM, clay and other minerals in over-mature marine shale: a case study of the Longmaxi shale from Southeast Chongqing, China. Mar. Petrol. Geol. 122, 104679. https://doi.org/10.1016/j.marpetgeo.2020. 104679.

Chen, S.B., Han, Y.F., Fu, C.Q., et al., 2016. Micro and nano-size pores of clay minerals in shale reservoirs: implication for the accumulation of shale gas. Sediment. Geol. 342, 180—190. https://doi.org/10.1016/j.sedgeo.2016.06.022.

Curtis, J.B., 2002. Fractured shale-gas systems. AAPG Bull. 86 (11), 1921–1938. https://doi.org/10.1306/61EEDDBE-173E-11D7-8645000102C1865D.

Do, D.D., Do, H.D., 2003. Adsorption of supercritical fluids in non-porous and porous carbons: analysis of adsorbed phase volume and density. Carbon 41 (9), 1777–1791. https://doi.org/10.1016/S0008-6223(03)00152-0.

Dubinin, M.M., Astakhov, V.A., 1971. Description of adsorption equilibria of vapors on zeolites over wide ranges of temperature and pressure. Adv. Chem. 102, 69–85. https://doi.org/10.1021/ba-1971-0102.ch044.

Fatah, A., Bennour, Z., Ben Mahmud, H., et al., 2020. A review on the influence of CO2/shale interaction on shale properties: implications of CCS in shales. Energies 13 (12), 3200. https://doi.org/10.3390/en13123200.

Feng, G.J., Zhu, Y.M., Chen, S.B., et al., 2020. Supercritical methane adsorption on shale over wide pressure and temperature ranges: implications for gas-in-place estimation. Energy Fuel. 34 (3), 3121–3134. https://doi.org/10.1021/acs.energyfuels.9b04498.

Gasparik, M., Bertier, P., Gensterblum, Y., et al., 2013. Geological controls on the methane storage capacity in organic-rich shales. Int. J. Coal Geol. 123, 34–51. https://doi.org/10.1016/j.coal.2013. 06.010.

Gong, J.M., Qiu, Z., Zou, C.N., et al., 2020. An integrated assessment system for shale gas resources associated with graptolites and its application. Appl. Energy 262, 114524. https://doi.org/10.1016/j.apenergy.2020.114524.

Gou, Q.Y., Xu, S., 2019. Quantitative evaluation of free gas and adsorbed gas content of Wufeng-Longmaxi shales in the Jiaoshiba area, Sichuan Basin, China. Adv. Geo-Energy Res. 3 (3), 258–267. https://doi.org/10.26804/ager.2019.03.04.

- Grieser, W.V., Bray, J.M., 2007. Identification of production potential in unconventional reservoirs. In: 2007 Production and Operations Symposium. SPE, 106623. https://doi.org/10.2118/106623-MS.
- Hao, F., Zou, H.Y., Lu, Y.C., 2013. Mechanisms of shale gas storage: implications for shale gas exploration in China. AAPG Bull. 97 (8), 1325–1346. https://doi.org/ 10.1306/02141312091.
- Huang, H.X., Li, R.X., Jiang, Z.X., et al., 2020. Investigation of variation in shale gas adsorption capacity with burial depth: insights from the adsorption potential theory. J. Nat. Gas Sci. Eng. 73, 103043. https://doi.org/10.1016/j.ingse.2019.103043.
- Huston, N.D., Yang, R.T., 1997. Theoretical basis for the Dubinin-Radushkevich (DR) adsorption isotherm equation. Adsorption 7 (3), 189–195. https://doi.org/10.1007/BF01650130.
- Jiang, W.B., Cao, G.H., Luo, C., et al., 2021. A composition-based model for methane adsorption of overmature shales in Wufeng and Longmaxi Formation, Sichuan Basin. Chem. Eng. J. 429, 130766. https://doi.org/10.1016/j.cej.2021.130766.
- Jiao, P.F., Yao, G.S., Zhou, S.W., et al., 2021. A comparative study of the micropore structure between the transitional and marine shales in China. Geofluids 5562532. https://doi.org/10.1155/2021/5562532.
- Klewiah, I., Berawala, D.S., Walker, H.C.A., et al., 2020. Review of experimental sorption studies of CO₂ and CH₄ in shales. J. Nat. Gas Sci. Eng. 73, 103045. https://doi.org/10.1016/j.ingse. 2019.103045.
- https://doi.org/10.1016/j.jngse. 2019.103045.

 Li, J., Wu, K.L., Chen, Z.X., et al., 2019. Effects of energetic heterogeneity on gas adsorption and gas storage in geologic shale systems. Appl. Energy 251, 113368. https://doi.org/10.1016/j.apenergy. 2019.113368.
- Li, W.B., Li, X., Zhao, S.X., et al., 2022. Evaluation on carbon isotope fractionation and gas-in-place content based on pressure-holding coring technique. Fuel 315, 123243. https://doi.org/10.1016/j. fuel.2022.123243.
- Liu, K.Q., Mehdi, O., Kong, L.Y., 2018. Multifractal characteristics of Longmaxi Shale pore structures by N2 adsorption: a model comparison. J. Petrol. Sci. Eng. 168, 330–341. https://doi.org/10.1016/j.petrol. 2018.04.072.
- Ma, K., Zhang, B., Wen, S.Y., et al., 2022. Quantitative characterization and controlling factors of shallow shale reservoir in taiyang anticline, zhaotong area, China. Minerals 12 (8), 998. https://doi.org/10.3390/min12080998.
- Ma, X.H., Wang, H.Y., Zhou, S.W., et al., 2021. Deep shale gas in China: geological characteristics and development strategies. Energy Rep. 1903–1914. https:// doi.org/10.1016/j.egyr.2021.03.043.
- Ma, Y.S., Cai, X.Y., Zhao, P.R., 2018. China's shale gas exploration and development: understanding and practice. Petrol. Explor. Dev. 45 (4), 589–603. https:// doi.org/10.1016/S1876-3804(18)30065-X (in Chinese).
- Memon, A., Li, A.F., Memon, B.S., et al., 2020. Gas adsorption and controlling factors of shale: review, application, comparison and challenges. Nat. Resour. Res. 30 (1), 827–848. https://doi.org/10.1007/s11053-020-09738-9.
- Merey, S., Sinayuc, C., 2018. Adsorption behavior of shale gas reservoirs. Int. J. Oil Gas Coal Technol. 17 (2), 172–188. https://doi.org/10.1504/IJOGCT.2018.10010677.
- Mosher, K., He, J.J., Liu, Y.Y., et al., 2013. Molecular simulation of methane adsorption in micro-and mesoporous carbons with applications to coal and gas shale systems. Int. J. Coal Geol. 109, 36–44. https://doi.org/10.1016/j.coal.2013.01.001.
- O'Neill, K.T., Birt, B., Hopper, T., 2021. Borehole measurements of adsorbed gas content in coals using stimulated diffusion nuclear magnetic resonance. Int. J. Coal Geol. 247, 103845. https://doi.org/10.1016/j.coal. 2021.103845.
- Saidian, M., Godinez, L.J., Prasad, M., 2016. Effect of clay and organic matter on nitrogen adsorption specific surface area and cation exchange capacity in shales (mudrocks). J. Nat. Gas Sci. Eng. 33, 1095–1106. https://doi.org/10.1016/ j.ingse.2016.05.064.
- Sakurovs, R., Day, S., Weir, S., et al., 2007. Application of a modified Dubinin-Radushkevich equation to adsorption of gases by coals under supercritical conditions. Energy Fuel. 21 (5), 992–997. https://doi.org/10.1021/ef0600614.
- Singh, P., Slatt, R., Borges, G., et al., 2009. Reservoir characterization of unconventional gas shale reservoirs: example from the Barnett Shale, Texas, USA. AAPG 61 (1), 15–31.

- Smith, D.M., Williams, F.L., 1984. Direct method of determining the methane content of coal a modification. Fuel 63, 425–427. https://doi.org/10.1016/0016-2361(84)90024-3
- Sun, S.S., Huang, S.P., Gomez-Rivas, E., et al., 2022. Characterization of natural fractures in deep-marine shales: a case study of the Wufeng and Longmaxi shale in the Luzhou Block Sichuan Basin, China. Front. Earth Sci. https://doi.org/10.1007/s11707-022-1021-2.
- Tang, X., Zhang, J.C., Wang, X.Z., et al., 2014. Shale characteristics in the southeastern Ordos Basin, China: implications for hydrocarbon accumulation conditions and the potential of continental shales. Int. J. Coal Geol. 128, 32–46. https://doi.org/ 10.1016/j.coal.2014.03.005.
- Ward, C.R., 2016. Analysis, origin and significance of mineral matter in coal: an updated review. Int. J. Coal Geol. 165, 1–27. https://doi.org/10.1016/i.coal.2016.07.014.
- Wang, M., Lun, Z.M., Zhao, C.P., et al., 2020. Influences of primary moisture on methane adsorption within lower silurian Longmaxi shales in the Sichuan Basin, China. Energy Fuel. 34, 10810–10824. https://doi.org/10.1021/acs.energyfuels.0c01932.
- Wang, R.Y., Gu, Y., Ding, W.L., et al., 2016. Characteristics and dominant controlling factors of organic-rich marine shales with high thermal maturity: a case study of the Lower Cambrian Niutitang Formation in the Cen'gong block, southern China. J. Nat. Gas Sci. Eng. 33, 81–96. https://doi.org/10.1016/j.jngse.2016.05.009.
- Wang, R.Y., Hu, Z.Q., Sun, C.X., et al., 2018. Comparative analysis of shale reservoir characteristics in the Wufeng-Longmaxi (O₃w-S₁I) and Niutitang (€₁n) Formations: a case study of the Wells JY1 and TX1 in southeastern Sichuan Basin and its periphery, SW China. Interpretation 6 (4), 31−45. https://doi.org/10.1190/INT-2018-0024.1.
- Xu, S., Gou, Q.Y., Hao, F., et al., 2019. Shale pore structure characteristics of the high and low productivity wells, Jiaoshiba shale gas field, Sichuan Basin, China: dominated by lithofacies or preservation condition? Mar. Petrol. Geol. 114, 104211. https://doi.org/10.1016/j.marpetgeo. 2019.104211.
- Yang, F., Xie, C.J., Ning, Z.F., et al., 2017. High-pressure methane sorption on dry and moisture-equilibrated shales. Energy Fuel. 31, 482–492. https://doi.org/ 10.1021/acs.energyfuels.6b02999.
- Yee, D., Seidle, J.P., Hanson, W.B., 1993. Gas sorption on coal and measurement of gas content (Chapter 9), 203-218. https://doi.org/10.1306/St38577C9.
- Zhang, H.M., Li, X.Z., Hu, Z.M., et al., 2022. Influence of particle size on the low-temperature nitrogen adsorption of deep shale in southern sichuan, China. Minerals 12 (3), 302. https://doi.org/10.3390/min12030302.
- Zhang, T.W., Ellis, G.S., Ruppel, S.C., et al., 2012. Effect of organic-matter type and thermal maturity on methane adsorption in shale-gas systems. Org. Geochem. 47, 120–131. https://doi.org/10.1016/j. orggeochem.2012.03.012.
- Zhou, S.W., Xue, H.Q., Ning, Y., et al., 2018. Experimental study of supercritical methane adsorption in Longmaxi shale: insights into the density of adsorbed methane. Fuel 211, 140–148. https://doi.org/10.1016/j.fuel.2017.09.065.
- Zhou, S.W., Zhang, D.X., Wang, H.Y., et al., 2019. A modified BET equation to investigate supercritical methane adsorption mechanisms in shale. Mar. Petrol. Geol. 105, 284–292. https://doi.org/10.1016/j.marpetgeo.2019.04.036.
- Zhou, S.W., Wang, H.Y., Li, B.B., et al., 2022. Predicting adsorbed gas capacity of deep shales under high temperature and pressure: experiments and modeling. Adv. Geo-Energy Res. 6 (6), 482–491. https://doi.org/10.46690/ager.2022.06.05.
- Zhu, H.J., Ju, Y.W., Huang, C., et al., 2020. Microcosmic gas adsorption mechanism on clay-organic nanocomposites in a marine shale. Energy 197, 117256. https:// doi.org/10.1016/j.energy.2020.117256.
- Zou, C.N., Yang, Z., Li, G.X., et al., 2022. Why can China realize the continental "shale oil revolution". J. Earth. SCI-China. 33, 1324–1327. https://doi.org/10.1007/s12583-022-1745-7.
- Zou, C.N., Zhao, Q., Cong, L.Z., et al., 2021. Development progress, potential and prospect of shale gas in China. Nat. Gas. Ind. 41 (1), 1–14. https://doi.org/10.3787/j.issn.1000-0976. 2021.01.001 (in Chinese).
- Zou, J., Rezaee, R., Xie, Q., et al., 2019. Characterization of the combined effect of high temperature and moisture on methane adsorption in shale gas reservoirs. J. Petrol. Sci. Eng. 182, 106353. https://doi.org/10.1016/j.petrol.2019.106353.